HHS Public Access

Author manuscript

Integr Biol (Camb). Author manuscript; available in PMC 2017 September 12.

Published in final edited form as:

Integr Biol (Camb). 2016 September 12; 8(9): 976–984. doi:10.1039/c6ib00082g.

Real-time Imaging and Quantitative Analysis of Doxorubicin Transport in a Perfusable Microvessel Platform

Max I. Bogorad[1,2] and **Peter C. Searson**[1,2,3]

[1]Institute for Nanobiotechnology, Johns Hopkins University, 3400 North Charles Street, Baltimore, MD 21218, USA

[2]Department of Materials Science and Engineering, Johns Hopkins University, 3400 North Charles Street, Baltimore, MD 21218, USA

[3]Sidney Kimmel Comprehensive Cancer Center, Johns Hopkins University, 401 N. Broadway Baltimore, MD 21287, USA

Abstract

Here we report on real-time imaging and quantitative analysis of solute transport in perfusable cylindrical microvessels formed from Madin-Darby Canine Kidney (MDCK) cells embedded in a collagen matrix. Fluorescence microscopy was used to image the kinetics of doxorubicin transport following injection. To assess the role of efflux pumps on transport, experiments were performed in microvessels formed from MDCK.2, MDCKII-w/t, and MDCKII-MDR1 cells. MDCKII-w/t and MDCKII-MDR1 showed significant doxorubicin accumulation in the cells, characteristic of the pharmacokinetics of doxorubicin. We present a model for doxorubicin transport that takes into account transport across the cell layer. These results demonstrate how real-time imaging of cell microvessels can be used to analyze the mechanisms of transport and distribution following systemic delivery.

Keywords

doxorubicin; permeability; transport; live-cell imaging; microvascular models

Introduction

The kinetics of solute transport across cell monolayers is complex, and often consists of multiple active transport processes in addition to passive diffusion. The transwell assay is widely used as an *in vitro* tool to assess transport of small molecules and potential therapeutics across biological barriers. In this assay a monolayer of cells is grown on a porous membrane that separates a top (apical) chamber from a bottom (basolateral) chamber. The molecule of interest is introduced into the apical chamber, and the apparent permeability P_{app} is calculated from the time-dependent concentration in the basolateral chamber. The transwell assay provides a quantitative measurement of solute permeability, and it is widely

correspondence: searson@jhu.edu, Peter Searson, 100 Croft Hall, Johns Hopkins University, 3400 North Charles Street, Baltimore, MD 21218. (410) 516 8774.

used with monolayers of epithelial and endothelial cells to model brain penetration and absorption of intravenously or orally administered drugs.[3–5]

Permeability is a global measure of transport rate but provides little insight into the details of the operating mechanisms. The purpose of this study is to demonstrate that mechanistic details of transport across biological barriers can be obtained from live cell imaging in a perfusable microvessel model with physiologically relevant geometry. Specifically, we report on the kinetics of doxorubicin transport in microvessels formed from three Madin-Darby Canine Kidney (MDCK) epithelial cell lines. MDCK cells form tight junctions, thereby minimizing paracellular transport. One of the cell lines used are genetically engineered versions of MDCKs that are routinely used to screen for substrates of the P-gp efflux pump, one of the main multidrug efflux transporters in brain microvascular endothelial cells.[6–8]

We investigate the kinetics of doxorubicin, a 543.52 Da small molecule anthracycline antibiotic, clinically used in multiple indications.[9] Doxorubicin is introduced systemically reaching a peak concentration in the blood plasma in the range of 40 – 60 mg m^{-2} (1.2 – 1.9 mM based on a body surface area of 1.8 m^2).[10] The pharmacokinetics of doxorubicin are characterized by a large distribution volume (typically > 250 – 1800 L), small area under the curve (0.5 – 3.8 mg h L^{-1}), high clearance rate (25 – 72 L h^{-1}), and short elimination half-time (about 24 h).[11, 12] These parameters highlight the fact that a significant amount of the drug is taken up in normal tissues during the first hour after administration. Doxorubicin is moderately fluorescent with an absorption peak around 475 nm and an emission peak at 600 nm.[13]

Fluorescence microscopy was used to capture the kinetics of doxorubicin transport after injection into the lumen of microvessels embedded in a collagen I matrix. Microvessels were formed with three cells lines: two wild type MDCK cell lines from different sources (MDCK.2 and MDCKII-w/t), and a MDCK line transfected to express the human P-gp efflux pump (MDCKII-MDR1). We first verified the integrity of the microvessels by measuring the permeability of Lucifer yellow, a molecule commonly used to validate endothelial monolayers in the transwell assay. Here we present a quantitative model for transport from which we can obtain rate constants from experimental measurements. These results show how real-time imaging of in *in vitro* microvessels can be used to analyze the mechanisms of transport and distribution following systemic delivery.

Materials and Methods

Fabrication of perfusable microvessels

The procedure for preparing a single microvessel embedded in a surrounding collagen matrix has been described in detail elsewhere[14] and is summarized in Supplementary Information.

Cell culture

MDCK.2 cells were obtained from ATCC (CRL-2936). MDCKII wild-type (MDCKII-w/t) and MDCKII-MDR1 cells were obtained from the Netherlands Cancer Institute

(Netherlands Cancer Institute, Amsterdam, The Netherlands). MDCK.2 cells were obtained at P80 and were used in experiments from P82 – P86. MDCKII-w/t cells were obtained at P9 and used from P11 – P14. MDCKII-MDR1 cells were obtained at P6 and used from P8 – P14. The growth media used for all cell types was Dulbecco's Modified Eagle Medium (Life Technologies), supplemented with $NaHCO_3$ (S-5761, Life Technologies), 10% fetal bovine serum (6140071, Life Technologies), and 1% penicillin streptomycin (15140122, Life Technologies).

Live cell imaging and time-lapse microscopy

The platform was mounted in a custom-built microscope stage in a live cell chamber on an inverted microscope (Nikon TE2000-U) and maintained at 37 °C and 5% CO_2. Phase contrast and fluorescence images were recorded for about 5 minutes to establish background conditions. Doxorubicin (200923, Santa Cruz) was then injected into the media reservoir to give a solute concentration of 10 μM, 100 μM, or 1 mM. Phase contrast and fluorescence images were recorded for 5 – 10 minutes to capture the initial increase in intensity when the solute reached the microvessel and the following steady state perfusion. The time for the solute to reach the microvessel from the media reservoir was about 30 s. Images were recorded at a frame rate of 20 s, selected to achieve maximum resolution for analysis of the transport kinetics and to avoid photobleaching. Fresh media was then injected into the media reservoir and imaging resumed for up to 2 h to capture the wash-out of the doxorubicin. Lucifer yellow (L-453, Life Technologies) was used as a negative control. In these experiments Lucifer yellow was injected into the media reservoir to give a concentration of 100 μM. Due to the slow kinetics, images were recorded at a frame rate of 60 s. Lucifer yellow is highly fluorescent with excitation/emission peaks at ~430/530 nm, while doxorubicin is moderately fluorescent with excitation/emission peaks at ~475/600 nm. All fluorescence images were obtained using filter set ET-Sedat Quad-band (8900, Chroma Technology Crop). Lucifer yellow was imaged using a 10X objective and excitation/emission filters ET402/ET525 at 60 ms exposure. Doxorubicin was imaged using a 20× objective and excitation/emission filters ET555/ET605 at 400 ms exposure and 4X gain. Details of image analysis are provided in Supplementary Information.

Kinetics of transcellular transport

The kinetics of transcellular transport of doxorubicin and Lucifer yellow were determined from analysis of phase contrast and fluorescence images. The permeability was determined using methods developed for similar experiments in resected vessels[15]. Prior to injection of the fluorescent solute, the microvessels were oriented in the field of view to image the microvessel and the surrounding extracellular matrix (ECM). The integrated fluorescence intensity in each frame, after background subtraction, was plotted versus time for analysis. Analysis was also performed by selecting an area immediately outside the cells to analyze the penetration of solute into the ECM.

Measurement of doxorubicin permeability in MDCKII-w/t cells using the transwell assay

Transwells (Corning, 24 well; 0.33cm^2 area, 0.4 μm pores) were pre-coated with rat tail collagen type I at a concentration of 10 μg cm^{-2}. MDCKII-w/t cells were seeded onto the transwell inserts at a density of 10^5 cells cm^{-2}. Hank's balanced salt solution (HBSS) was

used in both apical and basolateral chambers. Once the cells reached confluence, 100 μL of 100 μM doxorubicin was introduced into the apical chamber. The transwell inserts were moved to wells with clean buffer every 10 minutes for 30 minutes. The doxorubicin concentration in each basolateral well was measured using HPLC (see Supplementary Information for details).

RESULTS

Overview

We have developed an *in vitro* platform to image and quantitatively analyze the kinetics of drug transport in perfusable, cylindrical microvessels embedded in extracellular matrix (Figure 1), recapitulating the distribution of the drug following systemic injection. Microvessels approximately 150 – 200 μm in diameter were formed from MDCK.2, MDCKII-w/t, or MDCKII-MDR1 cells. Following injection of doxorubicin or Lucifer yellow into the media reservoir, the fluorescence intensity increased rapidly in the lumen as the concentration reached a steady state value (**see** Supplementary Videos S1 **and S2**). Introduction of the solute was followed by slow transport across the cell monolayer and diffusion into the extracellular matrix (ECM). Unless otherwise stated, all experiments were performed at a shear stress of 2 dyne cm^{-2}. We first show results and quantitative analysis from epifluorescence microscopy and then provide a comparison to confocal microscopy.

Transcellular transport was quantitatively assessed from analysis of fluorescence images from the movies (Figure 1e–h). The apparent permeability P_{app} (cm s^{-1}) of a solute across an endothelial monolayer in a cylindrical microvessel with diameter d is given by:[16]

$$P_{\mathrm{app}}=\frac{1}{\Delta I}\frac{dI}{dt}\frac{d}{4} \quad (1)$$

where ΔI is the initial increase in fluorescence intensity due to injection of the solute in the lumen of the microvessel and dI/dt is the slope at longer times. P_{app} describes the overall rate of solute transport from the lumen to the ECM. This method, originally developed for measurement of permeability in isolated vessels (Figure 1i),[15–19] has also been used in microvessel models.[14, 20–24] The fluorescence intensity is measured from a region of interest including the lumen, cells, and ECM (Figure 2h). As we show below, the fluorescence intensity includes contributions from the lumen, the cells, and the ECM. To separate the contribution from solute accumulation in the cells, we also calculate the permeability where the dI/dt term is determined from the fluorescence intensity in the ECM alone (Figure 2h). In this case the region of interest extended from a point immediately outside the cells, as determined from analysis of the phase contrast images.

Permeability of Lucifer yellow

First we describe the transcellular transport of Lucifer yellow. Lucifer yellow is a fluorescent molecule widely used to assess the integrity of endothelial monolayers in the transwell assay prior to measurement of the solute of interest.[25] Fluorescence images of microvessels following injection of Lucifer yellow (Supplementary Video S1 **and** Figure 2) show very

low intensity in the ECM. The total fluorescence intensity determined from the images shows a fast initial increase corresponding to the introduction into the lumen, followed by a subsequent linear increase corresponding to transport across the cells and diffusion into the ECM (Figure 3a). The fluorescence intensity in the ECM alone increases linearly with time for the three different cell lines (Figure 3b). In cylindrical PDMS tubes where we would expect negligible permeability, the fluorescence intensity outside the tubes does not increase over a period of 1 hour (see Supplementary Information).

The permeability of Lucifer yellow calculated from the total intensity (lumen and ECM) and ECM alone were almost identical, with values in the range 3×10^{-7} to 7×10^{-7} cm s^{-1} (Figure 4a). There was no statistical difference in the values for permeability obtained from the three cell lines. In the transwell assay, values of Lucifer yellow permeability less than 1×10^{-6} cm s^{-1} are used to confirm the integrity of MDCK monolayers.[26]

There are three main differences between our model and the transwell assay: curvature, substrate stiffness, and shear stress. The curvature (1/r) of our microvessels is relatively small and hence we would not expect significant differences compared to the 2D monolayer in the transwell assay. Larger differences may be obtained in capillaries where the curvature is much higher.[27] In the transwell assay, cells are seeded on a stiff collagen-coated porous membrane, whereas in our model, cells are seeded on a 3D collagen gel. Finally, transwell measurements are performed under static conditions whereas our measurements were performed at a low shear stress of 2 dyne cm^{-2}. The similarity in permeability suggests that these differences are small.

Permeability of doxorubicin

Having validated the barrier properties of the microvessels by measuring the permeability of Lucifer yellow, we next consider the kinetics of doxorubicin transport.

The kinetics of doxorubicin transport were strongly dependent on the cell type (Figure 2). The phase contrast and fluorescence images following injection of doxorubicin show accumulation in the cells for the MDCKII-w/t and, to a lesser extent, in the MDCKII-MDR1 cells. In contrast, there is no evidence of accumulation in the MDCK.2 cells.

The total fluorescence intensity (lumen + cells + ECM) for microvessels formed with the MDCK.2 cells increased linearly with time, but at a much slower rate than for microvessels formed with the MDCKII-w/t and MDCKII-MDR1 cells (Figure 3c). The fluorescence intensity for MDCKII-w/t microvessels increased more rapidly than MDCKII-MDR1 microvessels, but both cell lines showed a deviation from linearity at longer times. As we show below, this is due to accumulation of doxorubicin in the cells. Deviation from linearity was more pronounced for microvessels formed with the MDCKII-MDR1 cells (Figure 3c).

The fluorescence intensity obtained from the ECM alone was linear with time for microvessels formed from all three cell lines (Figure 3d). The phase contrast and fluorescence overlays (Figure 2) for the MDCKII-w/t and MDCKII-MDR1 microvessels clearly show increased intensity in the cells. This effect is described in more detail below.

The permeability coefficients for doxorubicin were obtained from analysis of the fluorescence intensity in the ECM (Figure 4b). The MDCKII-w/t microvessels had the highest average permeability of $10 \pm 0.87 \times 10^{-6}$ cm s^{-1}, while the transfected MDCKII-MDR1 microvessels had the lowest average permeability of $3.7 \pm 0.53 \times 10^{-6}$ cm s^{-1}. The MDCK.2 microvessels had an intermediate permeability of $5.2 \pm 1.9 \times 10^{-6}$ cm s^{-1}. The lower permeability ($p < 0.01$) for MDCKII-MDR1 microvessels compared to the MDCKII-w/t microvessels indicates that doxorubicin is a substrate of the P-gp efflux pump. The permeability of doxorubicin in MDCKII-w/t microvessels ($10 \pm 0.87 \times 10^{-6}$ cm s^{-1}) is very close to the value of $12.4 \pm 0.05 \times 10^{-6}$ cm s^{-1} obtained for MDCKII-w/t cells obtained using the transwell assay ($p = 0.15$) providing further evidence for the validity of the approach.

Influence of concentration on permeability

To assess the influence of doxorubicin concentration on transport we investigated the dependence of permeability on concentration in microvessels formed from MDCKII-MDR1 cells. The permeability of doxorubicin increased with increasing concentration (Figure 4c). On increasing the concentration from 10 μM to 100 μM, the average permeability increased from $0.32 \pm 0.23 \times 10^{-6}$ cm s^{-1} to $3.7 \pm 0.53 \times 10^{-6}$ cm s^{-1}, a factor of 11.7. On increasing the concentration from 100 μM to 1 mM, the permeability increased to $9.7 \pm 0.94 \times 10^{-6}$ cm s^{-1}, a factor of 2.6.

Influence of shear stress on permeability

In vivo, renal tubular epithelial cells (from which MDCKs are derived) experience a fluid shear stress that varies with urinary flow rate, and has been estimated in the range of 0.2 – 20 dyne cm^{-2}. Shear stress has been shown to regulate tight junction formation in renal epithelial cells, therefore we assessed the influence of shear stress on permeability in MDCK-MDR1 microvessels at 2 and 9 dyne cm^{-2}. The average permeabilities were 5.2×10^{-6} cm s^{-1} and 6.3×10^{-6} cm s^{-1}, respectively (Figure 4d). We found no statistically significant difference between the two values.

Doxorubicin accumulation in the cells

On injection of 100 μM doxorubicin, both MDCKII-w/t and MDCK-MDR1 microvessels showed significant accumulation of doxorubicin in the cells, while the MDCK.2 microvessels showed no significant accumulation (Figure 2). This is reflected in the plots of fluorescence intensity for MDCKII-w/t and MDCKII-MDR1 microvessels where the total intensity (lumen, cells, and ECM) (Figure 3c) increases much more rapidly than the intensity in the ECM alone (Figure 3d). Therefore the apparent permeability obtained from analysis of the fluorescence intensity of the lumen and ECM using the conventional method is significantly larger than the actual permeability obtained from analysis of the intensity from the ECM.

Drug accumulation is related to the fact that doxorubicin is a weakly basic molecule with a pK_a of 8.3,[31] and hence neutral doxorubicin (D^0) becomes protonated (D^+) in neutral or weakly acidic environments. Although neutral doxorubicin can passively diffuse across cell membranes, protonated doxorubicin has extremely low permeability due to the excess

charge,[32] and hence accumulates within the cell. Here our focus is on developing a general model for quantitative analysis of transport and drug accumulation. A more detailed model taking into account passive membrane transport, dissociation and efflux is presented in Supplementary Information.

The accumulation of doxorubicin in the cells was quantitatively assessed from analysis of phase contrast and fluorescence images. First, the location of the inner and outer vessel wall was determined from the phase contrast images. Next, we obtained line scans (one pixel wide) of the intensity profile along the center of the vessel wall from the fluorescence images (Figure 5a, b). At each time point, we subtracted the intensity profile at $t = 0$ immediately prior to injection of the drug and normalized to the average fluorescence intensity in the lumen at the first time point ($t = 20$ s). Due to the cylindrical geometry of the microvessels, the epifluorescence intensity is dependent on the position. Therefore, to normalize the intensity in the vessel wall we determine the lumen intensity at a point just inside (10 μm) the vessel wall where the height is the same as the vessel wall (see Supplementary Information). The intensity profiles in the vessel wall at 60, 120, and 300 s and along lumen (after background subtraction and normalization) are plotted for an MDCKII-MDR1 microvessel in Figure 5b. These plots show that the fluorescence intensity in the vessel wall exceeds that of the lumen after 300 seconds (Figure 5b).

The use of epifluorescence images for this analysis relies on the assumption that the intensity in the cells in the vessel wall is correctly normalized to the intensity in the vessel lumen. To validate the analysis using epifluorescence microscopy, we performed experiments where we simultaneously imaged MDCKII-MDR1 vessels following injection of doxorubicin using epifluorescence and confocal microscopy. We plotted the distribution of normalized pixel intensity in the vessel wall in both cases (Figure 5c). With increasing time following injection of doxorubicin, both distributions become broader and shift to higher average intensities. While the pixel intensity distributions obtained from confocal images are generally broader, the mean intensities at each time point are almost identical to values obtained from epifluorescence microscopy. These results show that drug accumulation in cells can be obtained from analysis of either epifluorescence or confocal microscopy images. Below we analyze drug accumulation in the cells from analysis of epifluorescence images.

The average normalized intensity at each time point (Figure 5c), which represents the accumulation of doxorubicin in the cells, is dependent on cell line. In contrast with MDCK.2 cells, the intensity in MDCKII-w/t and MDCKII-MDR1 cells increased above the concentration in the lumen, highlighting the significant accumulation of doxorubicin within the cells.

Modeling doxorubicin transport

Having developed a method for quantitative measurement of the time dependent accumulation of doxorubicin in the cells that form the vessel wall (Figure 5d), we next develop a model for mechanistic analysis of the transport processes. Our microvessel is a three-compartment system with: (1) the lumen, (2) vessel wall (consisting of epithelial cells), and (3) the ECM (Figure 5e). In the most general case, we can divide solute transport

into two processes: net solute entry into the cells (k_{in}) and net solute exit from the cells (k_{out}), where k_{in} and k_{out} are the corresponding first order rate constants with units of cm s^{-1}. Solute may enter the cells from the lumen or from the ECM, however the ECM is large enough that we can neglect the latter contribution. Likewise, solute exit from the cells includes transport back into the lumen (k_1) or forward into the ECM (k_2). In the absence of active transport or other asymmetric transport mechanisms (i.e. efflux), k_1 and k_2 are equal and exactly one half of k_{out}. Thus, solute transport can be described by three rate constants (cm s^{-1}): k_{in}, k_1, and k_2, where the first term describes solute entry into the cells from the lumen and the second two terms describe solute exit from the cells (Figure 5e). These apparent rate constants represent the overall rates of transport into and out of the microvessel and do not distinguish between transport mechanisms (e.g. diffusion, binding, dissociation, etc.). Having defined these constants, we can write the rate equation describing doxorubicin accumulation in the cells:

$$\frac{d[\mathrm{Dox}]_{\mathrm{cells}}}{dt}\Delta r = k_{\mathrm{in}}[\mathrm{Dox}]_{\mathrm{lumen}} - k_{\mathrm{out}}[\mathrm{Dox}]_{\mathrm{cells}} \quad (2)$$

where $[Dox]_{cells}$ is the time dependent concentration of doxorubicin in the cells, $[Dox]_{lumen}$ is the (constant) concentration of doxorubicin in the lumen, Δr is the thickness of the cell monolayer that defines the vessel wall, and $k_{out} = k_1 + k_2$. This model assumes a uniform cylindrical cell layer as shown in Figure 5e, where the volume of the cells per unit length = $2\pi r\Delta r$ and the surface area of the cells per unit length of vessel = $2\pi r$. The solution to equation (2) is given by:

$$[\mathrm{Dox}]_{\mathrm{cells}}(t) = \frac{k_{\mathrm{in}}}{k_{\mathrm{out}}}\left(1+\exp\left(-\frac{k_{\mathrm{out}}t}{\Delta r}\right)\right)[\mathrm{Dox}]_{\mathrm{lumen}} \quad (3)$$

Note that at steady state the doxorubicin concentration in the cells is a maximum and is given by:

$$[\mathrm{Dox}]_{\mathrm{cells}} = \frac{k_{\mathrm{in}}}{k_{\mathrm{out}}}[\mathrm{Dox}]_{\mathrm{lumen}} \quad (4)$$

This equation shows that accumulation within the cells is dependent on the ratio k_{in}/k_{out}. Least squares fits of equation (3) to the experimental data were used to obtain values for k_{in} and k_{out} (Figure 5d). The excellent fits for all three cell lines confirm the applicability of the model.

To obtain the relative contributions of k_1 and k_2 to the total forward transport into the ECM, we consider the ECM compartment, where the accumulation of solute is given by:

$$V_e\frac{d[\mathrm{Dox}]_{ECM}}{dt} = k_2 A_c[\mathrm{Dox}]_{\mathrm{cells}} \quad (5)$$

where V_e is the volume of the ECM in the chamber and A_c is the surface area of the cell-lumen interface.

At steady state, $[Dox]_{cells}$ can be replaced with the expression from equation (4):

$$V_e \frac{d[\mathrm{Dox}]_{ECM}}{dt} = k_2 A_c \frac{k_{\mathrm{in}}}{k_{\mathrm{out}}} [\mathrm{Dox}]_{\mathrm{lumen}} \quad (6)$$

The apparent permeability (P_{app}) is defined as the net solute transport rate into the ECM chamber normalized by the surface area through which the flow takes place and the concentration in the lumen:[33–36]

$$P_{\mathrm{app}} = V_e \frac{d[\mathrm{Dox}]_{ECM}}{dt} \frac{1}{A_c [\mathrm{Dox}]_{\mathrm{lumen}}} \quad (7)$$

Comparing equations (6) and (7) it is evident that k_2 can be written in terms of the experimentally determined constants k_{in}, k_{out}, and P_{app}:

$$k_2 = k_{\mathrm{out}} \frac{P_{\mathrm{app}}}{k_{\mathrm{in}}} \quad (8)$$

$$k_1 = k_{\mathrm{out}} - k_2 = k_{\mathrm{out}} \left(1 - \frac{P_{\mathrm{app}}}{k_{\mathrm{in}}}\right) \quad (9)$$

We can substitute the measured values of P_{app} and the fitted values for k_{in} and k_{out} to determine k_1 and k_2, and these values are tabulated in Figure 5f. Although the constants themselves do not describe any one physical process, they do have physical implications. For example, the solute efflux ratio can be easily calculated from k_1 and k_2 (Efflux Ratio = k_1/k_2) without knowledge of the underlying transport mechanisms (see Supplementary Information). The efflux ratio of 3.8 obtained from the MDCKII-MDR1 vessels (compared to 1.1 in MDCKII-w/t and 1.0 in the MDCK.2 vessels) is consistent with the fact that MDCKII-MDR1 cells are transfected to express P-gp pumps that are polarized to the luminal surface resulting in faster transport to the luminal compartment compared to the ECM compartment (Figure 5e).

Discussion

The transport of Lucifer yellow across MDCK.2, MDCKII-w/t, and MDCKII-MDR1 microvessels is consistent with ideal transcellular transport by passive diffusion with negligible accumulation or trapping in the cells, and negligible influence from efflux pumps. The value of the permeability was independent of position along the length of the microvessel confirming the uniformity. There was no statistical difference in permeability

across the three cell lines, further confirming that the mechanism is the same in all cases. The low permeability of Lucifer yellow verifies the integrity of the microvessels, and demonstrates that the 2D transwell assay can be translated into a 3D cylindrical geometry. The *in vitro* platform allows real-time imaging of the distribution of the drug over time.

The permeability of doxorubicin (100 μM) across the microvessels was strongly dependent on the MDCK cell line, with values of $10 \pm 0.87 \times 10^{-6}$ cm s^{-1}, $3.7 \pm 0.53 \times 10^{-6}$ cm s^{-1}, and $5.2 \pm 1.9 \times 10^{-6}$ cm s^{-1} for MDCKII-w/t, MDCKII-MDR1, and MDCK.2 cells, respectively. The permeability of doxorubicin in MDCKII-w/t microvessels ($10 \pm 0.87 \times 10^{-6}$ cm s^{-1}) and obtained from the transwell assay ($12.4 \pm 0.05 \times 10^{-6}$ cm s^{-1}) are very close, indicating that the experimental differences in curvature, substrate stiffness, and shear stress are not significant.

Doxorubicin concentration

The doxorubicin permeability in MDCKII-MDR1 microvessels increased by a factor of 11.7 with an increase in doxorubicin concentration from 10 to 100 μM, but then increased by a factor of 2.6 when the concentration was further increased to 1 mM (Figure 4c). A similar order of magnitude increase in doxorubicin permeability on increasing the concentration from 10 μM to 100 μM can be inferred from different studies of doxorubicin permeability in CaCo-2 cells: a doxorubicin permeability of $1 \times 10^{-6} – 3 \times 10^{-6}$ cm s^{-1} was reported at a concentration of 10 μM,[37, 38] and a value of 14×10^{-6} cm s^{-1} was reported at a concentration of 100 μM.[39] The permeability values of several drugs that are P-gp substrates show a sigmoidal dependence on drug concentration in MDCKII-MDR1 and CaCo-2 cells.[40] At low concentrations, the permeability is independent of concentration but then increases by up to a factor of 10 over a concentration range of about an order of magnitude before reaching a plateau at higher concentrations. The transition typically occurs at solute concentrations from 1 – 100 μM,[40] similar to the results reported here.

Shear stress

To assess the influence of shear stress we measured the doxorubicin permeability in MDCK-MDR1 microvessels at a concentration of 100 μM and at shear stresses of 2 and 9 dyne cm^{-2}, representing the upper limit with the current design. There was no significant difference in permeability at high and low shear stress. These results suggest that shear stress does not significantly influence doxorubicin transport in MDCK cells.

Doxorubicin Transport

Significant doxorubicin accumulation, above the concentration in the lumen, was observed in MDCKII-w/t and MDCK-MDR1 microvessels. In the literature, incubation of HL-60 leukemia cells with doxorubicin resulted in accumulation that was 1.7 fold higher than in cells transfected with the MDR1 gene,[42] similar to the difference between our observed accumulation in MDCKII-w/t and MDCKII-MDR1 cells after 600 seconds (1.9-fold difference). Doxorubicin transport (and solute transport in general) can be described in terms of a model with apparent rate constants for solute transport into the cells (k_{in}) and out of the cells (k_1, k_2) that make up the vessel. From the fits to our data and the measured permeability we obtain values for these rate constants. The estimated efflux ratio, calculated

from the ratio of k_1 to k_2, is elevated in the MDCKII-MDR1vessels (ER = 3.8) compared to the wild type vessels (MDCKII-w/t = 1.1, and MDCK.2 = 1.0), suggesting a polarization of efflux transporters in the MDCKII-MDR1 vessels. These results show that *in vitro* cell microvessel models can be used for imaging and quantitative analysis of drug transport in microvessels.

Summary

We have used an *in vitro* cell microvessel with MDCK.2, MDCKII-w/t, and MDCKII-MDR1 cells to study the transcellular transport of doxorubicin. *In vitro* platforms for drug discovery and screening of potential therapeutics are key for drug development. Real-time imaging of the distribution of a drug in an *in vitro* cell microvessel platform provides an additional tool for quantitative mechanistic analysis of transport from the blood to surrounding tissues. Additionally, since MDCK cells are widely used in *in vitro* models to study the blood-brain-barrier, MDCK microvessels may be particularly useful as an additional tool for studying brain penetration.

Supplementary Material

Refer to Web version on PubMed Central for supplementary material.

Acknowledgments

The authors would like to thank Dr. Charlene Dawidczyk for assistance with HPLC sample preparation and data collection. The authors gratefully acknowledge support from the American Heart Association (15GRNT25090122), DTRA (HDTRA1-15-1-0046), and NIH (R01CA170629).

References

1. Aird WC. Journal of Thrombosis and Haemostasis. 2005; 3:1392–1406. [PubMed: 15892866]
2. Aird WC. Circulation Research. 2007; 100:158–173. [PubMed: 17272818]
3. Artursson P, Palm K, Luthman K. Advanced Drug Delivery Reviews. 2001; 46:27–43. [PubMed: 11259831]
4. Summerfield SG, Read K, Begley DJ, Obradovic T, Hidalgo IJ, Coggon S, Lewis AV, Porter RA, Jeffrey P. Journal of Pharmacology and Experimental Therapeutics. 2007; 322:205–213. [PubMed: 17405866]
5. Cecchelli R, Berezowski V, Lundquist S, Culot M, Renftel M, Dehouck MP, Fenart L. Nature Reviews Drug Discovery. 2007; 6:650–661. [PubMed: 17667956]
6. Pastan I, Gottesman MM, Ueda K, Lovelace E, Rutherford AV, Willingham MC. Proceedings of the National Academy of Sciences. 1988; 85:4486–4490.
7. Yang Z, Horn M, Wang J, Shen DD, Ho RJ. AAPS PharmSci. 2004; 6:77–85.
8. Cordon-Cardo C, O'Brien JP, Casals D, Rittman-Grauer L, Biedler JL, Melamed MR, Bertino JR. Proceedings of the National Academy of Sciences. 1989; 86:695–698.
9. Oktay Tacar PS, Dass Crispin. Journal of Pharmacy and Pharmacology. 1989; 65:157–170. [PubMed: 23278683]
10. Vasey PA, Kaye SB, Morrison R, Twelves C, Wilson P, Duncan R, Thomson AH, Murray LS, Hilditch TE, Murray T. Clinical Cancer Research. 1999; 5:83–94. [PubMed: 9918206]
11. Piscitelli SC, Rodvold KA, Rushing DA, Tewksbury DA. Clinical Pharmacology & Therapeutics. 1993; 53:555–561. [PubMed: 8387903]
12. Erttmann R, Erb N, Steinhoff A, Landbeck G. Journal of Cancer Research and Clinical Oncology. 1988; 114:509–513. [PubMed: 3182911]

13. Dai X, Yue Z, Eccleston ME, Swartling J, Slater NKH, Kaminski CF. Nanomedicine: Nanotechnology, Biology and Medicine. 2008; 4:49–56.
14. Wong AD, Searson PC. Cancer Research. 2014; 74:4937–4945. [PubMed: 24970480]
15. Yuan Y, Chilian WM, Grainger HJ, Zawieja DC. American Journal of Physiology. 1993; 264:543–552.
16. Huxley FECVH, Adamson RH. American Journal of Physiology. 1983; 252:188–197.
17. Yuan Y, Granger HJ, Zawieja DC, Chilian WM. American Journal of Physiology-Heart and Circulatory Physiology. 1992; 263:H641–H646.
18. Yuan Y, Granger HJ, Zawieja DC, DeFily DV, Chilian WM. American Journal of Physiology-Heart and Circulatory Physiology. 1993; 264:H1734–H1739.
19. Yuan Y, Huang Q, Wu HM. American Journal of Physiology-Heart and Circulatory Physiology. 1997; 272:H1437–H1443.
20. Chrobak KM, Potter DR, Tien J. Microvasc Res. 2006; 71:185–196. [PubMed: 16600313]
21. Price GM, Tien J. Methods Mol Biol. 2011; 671:281–293. [PubMed: 20967637]
22. Price GM, Wong KH, Truslow JG, Leung AD, Acharya C, Tien J. Biomaterials. 2010; 31:6182–6189. [PubMed: 20537705]
23. Leung AD, Wong KH, Tien J. Journal of Biomedical Materials Research Part A. 2012; 100:1815–1822. [PubMed: 22489049]
24. Wong KH, Truslow JG, Tien J. Biomaterials. 2010; 31:4706–4714. [PubMed: 20303168]
25. Hidalgo, Ismael J.; Raub, TJ.; Borcchardt, RT. Gastroenterology. 1989; 96:736–749. [PubMed: 2914637]
26. Irvine JD, Takahashi L, Lockhart K, Cheong J, Tolan JW, Selick HE, Grove JR. Journal of Pharmaceutical Sciences. 1999; 88:28–33. [PubMed: 9874698]
27. Ye M, Sanchez HM, Hultz M, Yang Z, Bogorad M, Wong AD, Searson PC. Scientific Reports. 2014; 4
28. Lipowsky HH, Kovalcheck S, Zweifach BW. Circ Res. 1978; 43:738–749. [PubMed: 709740]
29. Kamiya A, Bukhari R, Togawa T. Bulletin of Mathematical Biology. 1984; 46:127–137. [PubMed: 6713148]
30. Davies PF, Mundel T, Barbee KA. Journal of Biomechanics. 1995; 28:1553–1560. [PubMed: 8666594]
31. Skovsgaard T. Biochemical Pharmacology. 1977; 26:215–222. [PubMed: 14644]
32. Frezard F, Garnier-Suillerot A. European Journal of Biochemistry. 1991; 196:483–491. [PubMed: 1672520]
33. Palumbo P, Picchini U, Beck B, van Gelder J, Delbar N, DeGaetano A. Journal of pharmacokinetics and pharmacodynamics. 2008; 35:235–248. [PubMed: 18351296]
34. Jung SJ, Choi SO, Um SY, Kim JI, Choo HYP, Choi SY, Chung SY. Journal of pharmaceutical and biomedical analysis. 2006; 41:469–475. [PubMed: 16460901]
35. Yazdanian M, Glynn SL, Wright JL, Hawi A. Pharmaceutical Research. 15:1490–1494. [PubMed: 9755906]
36. Liang E, Proudfoot J, Yazdanian M. Pharmaceutical Research. 17:1168–1174. [PubMed: 11145220]
37. Batrakova EV, Li S, Miller DW, Kabanov AV. Pharmaceutical Research. 2008; 16:1366–1372. [PubMed: 10496651]
38. Ingels F, Beck B, Oth M, Augustijns P. International Journal of Pharmaceutics. 2004; 274:221–232. [PubMed: 15072798]
39. Shiyin Y. Pharmaceutical Research. 1997; 14:763–766. [PubMed: 9210194]
40. Yoshiyuki Shirasaka TS, Yamashita Shinji. Journal of Pharmaceutical Sciences. 2008; 88:553–565. [PubMed: 17828734]
41. Turitto V. Progress in Hemostasis and Thrombosis. 1982; 6:139. [PubMed: 6762611]
42. Seynhaeve AL, Dicheva BM, Hoving S, Koning GA, ten Hagen TL. Journal of Controlled Release. 2013; 172:330–340. [PubMed: 24012486]

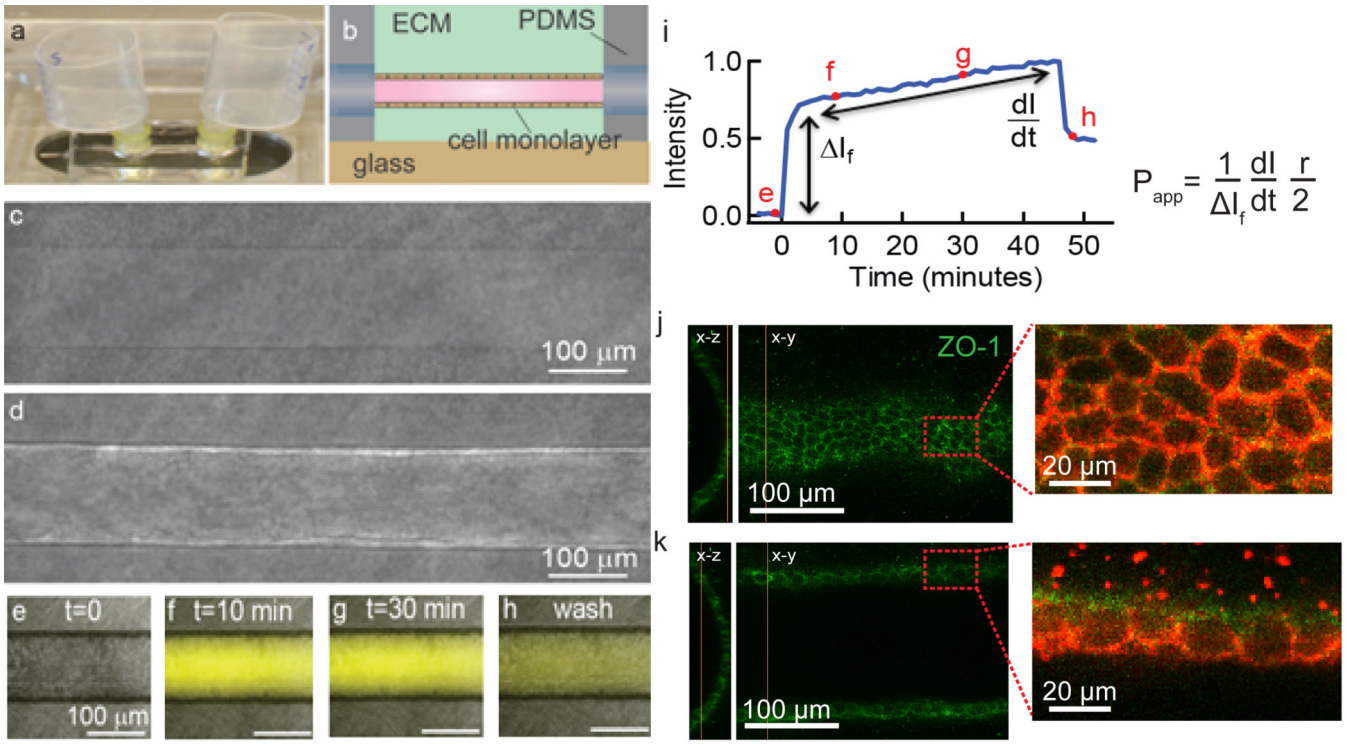

Fig. 1.

Imaging and analysis of transcellular transport in an *in vitro* platform. (a) The microvessel is located in an optically transparent PDMS housing with reservoirs for perfusion with media. (b) Schematic illustration showing the location of the microvessel within the PDMS housing. (c) Phase contrast image of a 150 μm diameter cylindrical channel embedded in a collagen matrix. (d) After seeding cells, a confluent monolayer is formed defining the lumen of the microvessel. (e–h) Phase contrast and fluorescence overlays of a microvessel following introduction of Lucifer yellow. (i) Normalized pixel intensity obtained from fluorescence images versus time following introduction of Lucifer yellow into the microvessel. The intensity is normalized to the maximum value. Following an initial increase, the intensity increases linearly as Lucifer yellow is transported across the cells and diffuses into the extracellular matrix. (j) Immunofluorescence images of the bottom of an MDCKII microvessel showing the tight junction network. (k) Immunofluorescence images at the equator of the microvessel show continuous ZO-1 and claudin-1 tight junction networks.

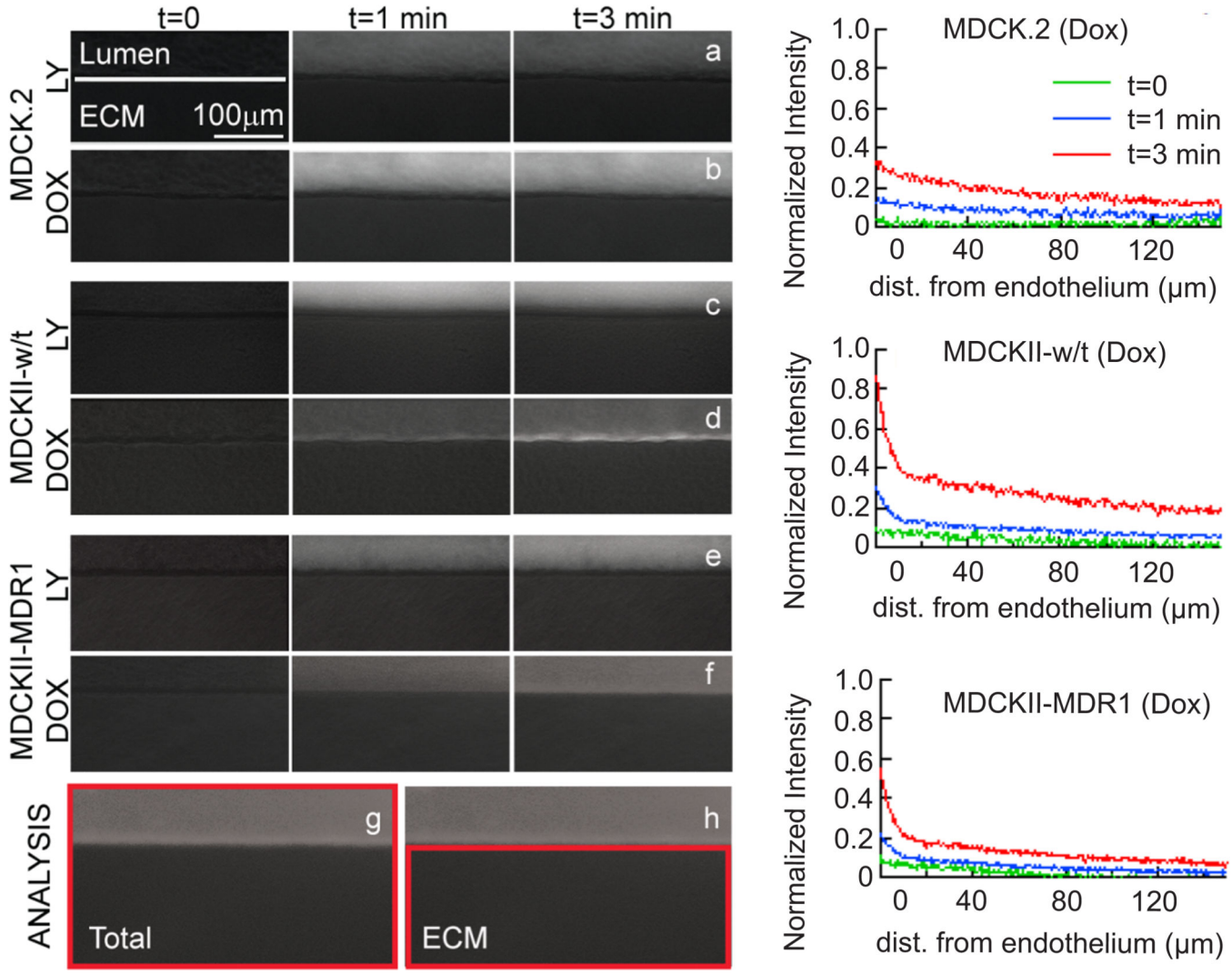

Fig. 2.

Doxorubicin and Lucifer yellow transport in microvessels. Overlays of phase contrast and fluorescence images of (a,b) MDCK.2 microvessels, (c,d) MDCKII-w/t microvessels, and (e,f) MDCKII-MDR1 microvessels on introduction of (a,c,e) Lucifer yellow and (b,d,f) doxorubicin. Microvessels were centered at the top of the image to optimize image analysis. The high fluorescence intensity in the cells for the MDCKII-w/t and MDCKII-MDR1 microvessels indicates significant uptake within the cells. There is no evidence of doxorubicin uptake in the MDCK.2 cells. The permeability was analyzed from images where the region of interest was defined as (g) lumen, cells, and ECM, or (h) ECM alone. Plots of fluorescence intensity versus distance normal to the microvessel axis are provided in Supplementary Information. (i–k) Normalized doxorubicin intensity profiles as a function of distance from the endothelium at t = 0, 1, and 3 minutes after injection in MDCK.2, MDCKII-w/t, and MDCKII-MDR1 vessels, respectively.

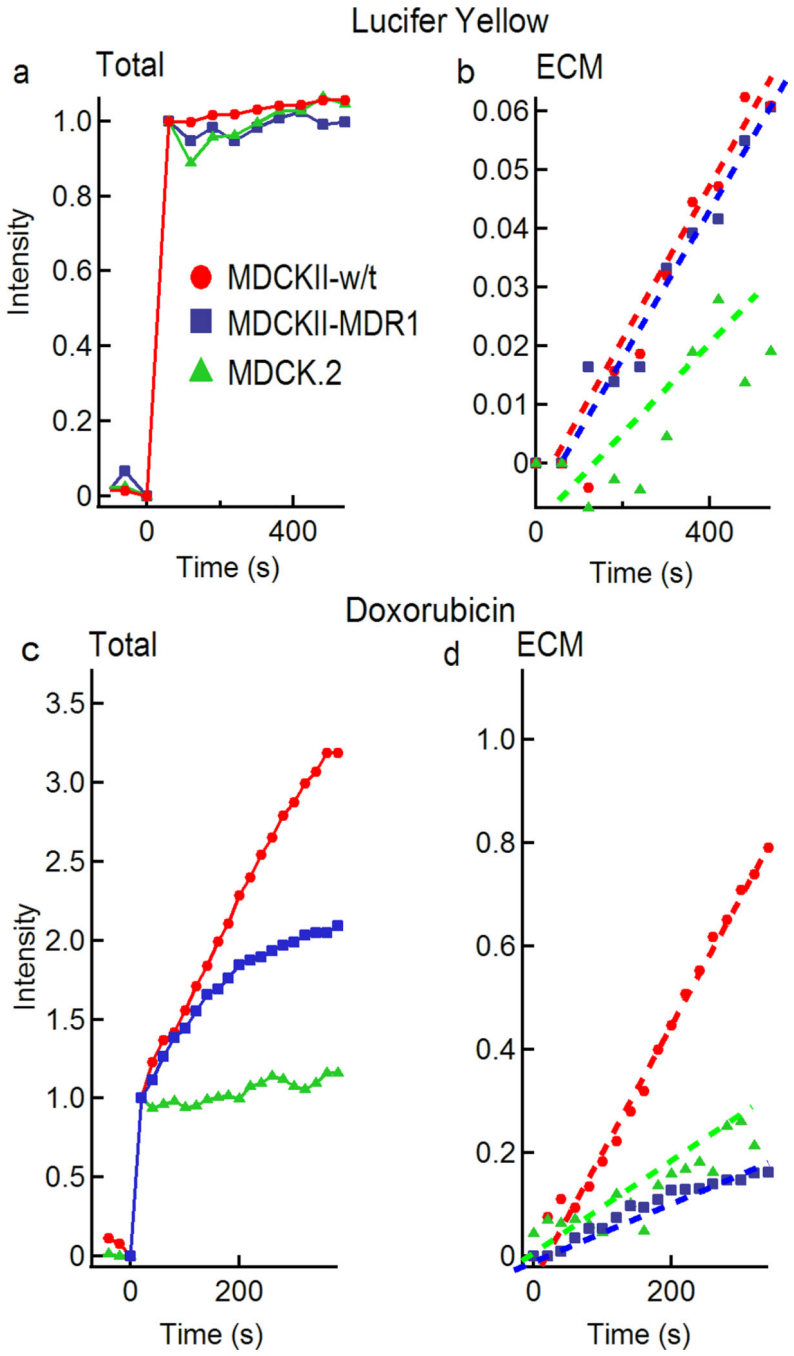

Fig. 3.

Normalized fluorescence intensity versus time for Lucifer yellow and doxorubicin in microvessels formed from MDCK.2, MDCKII-w/t, or MDCKII-MDR1 cells. (a) Total fluorescence intensity (lumen + ECM) and (b) fluorescence intensity in the ECM following injection of 100 μM Lucifer yellow. (c) Total fluorescence intensity (lumen + ECM) and (d) fluorescence intensity in the ECM following injection of 100 μM doxorubicin. All plots are normalized to the total intensity in the lumen.

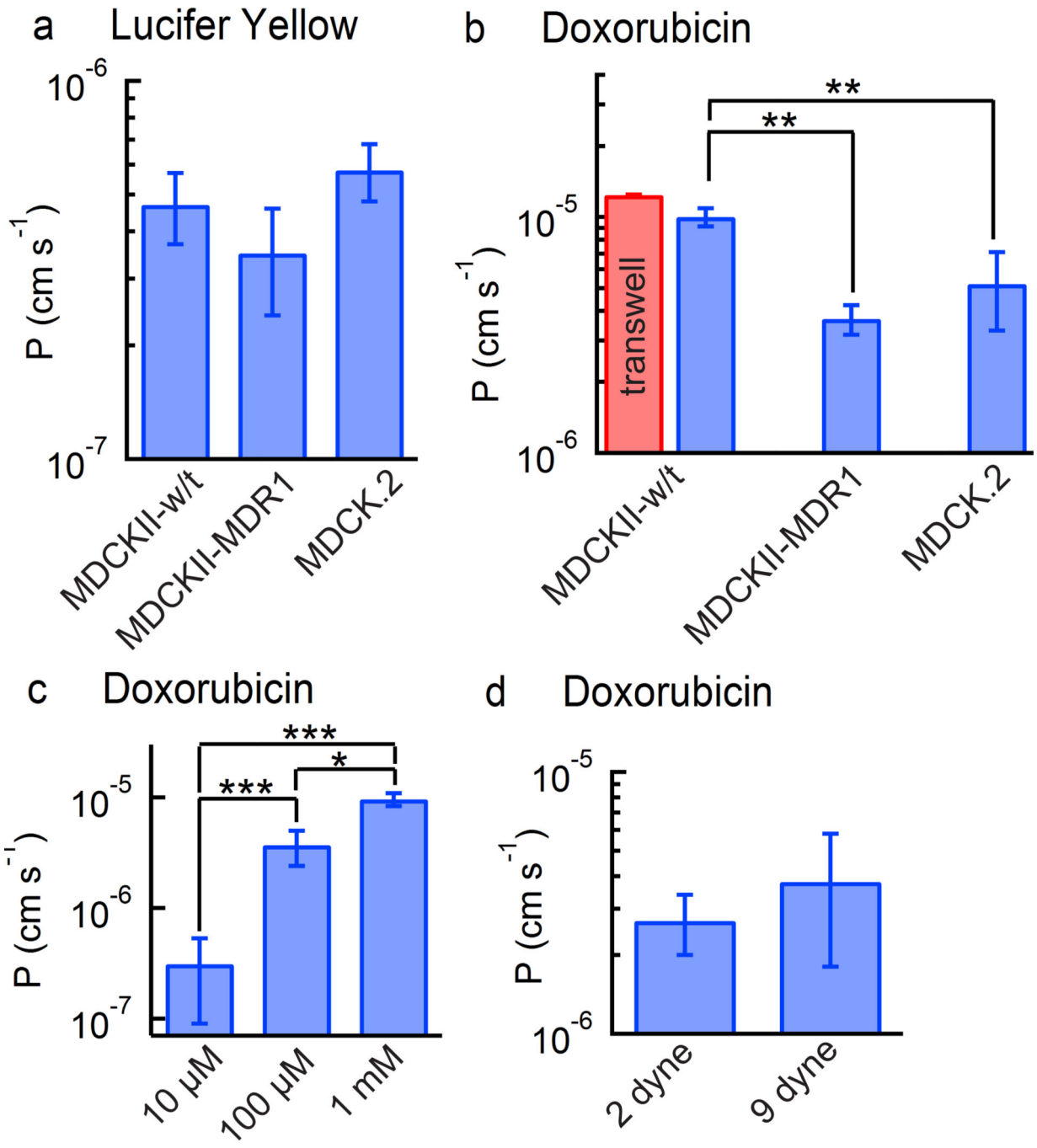

Fig. 4.

Permeability of doxorubicin and Lucifer yellow in microvessels formed from MDCK.2, MDCKII-w/t, or MDCKII-MDR1 cells. In all cases the permeability was calculated from the change in fluorescence intensity in the ECM. (a) Permeability for Lucifer yellow (c = 100 μM) across MDCK.2, MDCKII-w/t, or MDCKII-MDR1 microvessels (N = 3). (b) Permeability for doxorubicin (c = 100 μM) across MDCK.2, MDCKII-w/t, or MDCKII-MDR1 microvessels (N = 3). (c) Permeability of doxorubicin in MDCKII-MDR1 microvessels at three different doxorubicin concentrations (N = 3). (d) Permeability of

doxorubicin in MDCKII-MDR1 microvessels at 2 dyne cm^{-2} and 9 dyne cm^{-2} (N = 3). Error bars represent standard error. Statistical significance was determined using a student's t-test test. *** $P \leq 0.001$, ** $P \leq 0.01$. * $P \leq 0.05$.

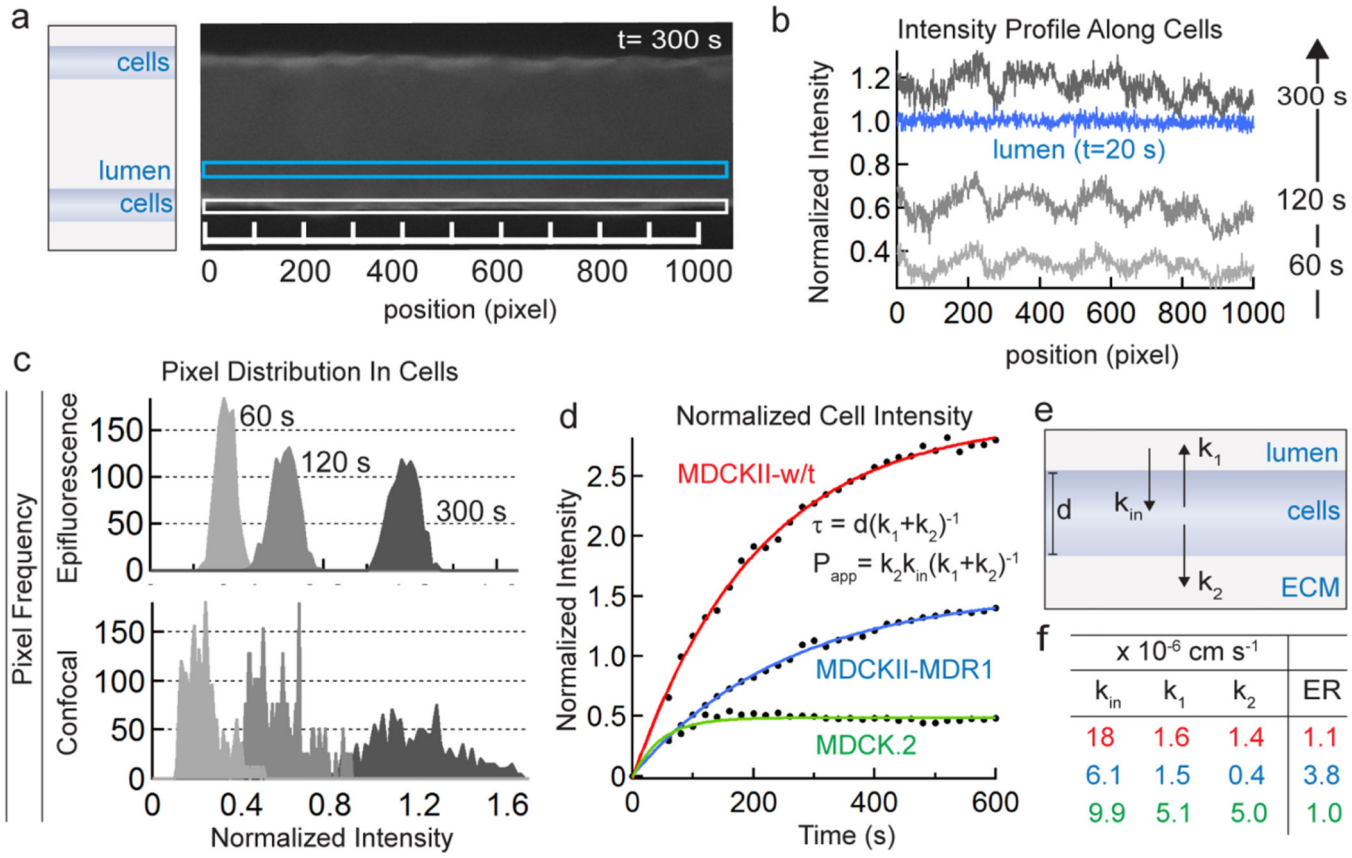

Figure 5.

Analysis of doxorubicin accumulation in cells following injection of 100 μM doxorubicin. (a) Fluorescence images of microvessels at each time point are used to obtain intensity profiles in the cells making up along vessel walls (white box) and in the lumen (blue box). (b) Representative intensity profiles along the cells at 60, 120, and 300 s and along lumen (after background subtraction and normalization) in an MDCKII-MDR1 microvessel. The cell intensity exceeds the lumen intensity after 300 seconds. (c) Representative pixel distributions along the cells at 60, 120, and 300 seconds from epifluorescence images (top) and confocal images (bottom). (d) The normalized intensity in the cells versus time for MDCK.2, MDCKII-w/t, and MDCKII-MDR1 microvessels. The average normalized fluorescence intensity in the cells at each time point was calculated from analysis of each frame using the sequential procedure described above. Fits for each cell line are shown. (e) Schematic illustration showing the kinetic model used to fit the data. k_{in} represents the rate constant for doxorubicin entry into the cells from the lumen, k_1 represents the rate constant for doxorubicin exit from the cells back to the lumen, and k_2 represents the rate constant for doxorubicin exit from the cells into the ECM. The rate constants have units of (cm s^{-1}). (f) Tabulated values for k_{in}, k_1, k_2, from the representative experiments shown (× 10^{-6} cm s^{-1}). Also tabulated is the calculated Efflux Ratio (ER) determined from the ratio k_1/k_2.